Functional Integration of New Hippocampal Neurons Following Insults to the Adult Brain is Determined by Characteristics of Pathological Environment

James C. Wood,[1,4,7] Johanna S. Jackson,[1,4,7] Katherine Jakubs,[1,4,6] Katie Z. Chapman,[1,4] Christine T. Ekdahl,[1,4,5] Zaal Kokaia,[3,4] Merab Kokaia,[2] and Olle Lindvall[1,4]

[1]Laboratory of Neurogenesis and Cell Therapy, and [2]Experimental Epilepsy Group, Wallenberg Neuroscience Center, [3]Laboratory of Neural Stem Cell Biology and Therapy, and [4]Lund Stem Cell Center, [5]Division of Clinical Neurophysiology, Lund University Hospital, SE-221 84 Lund, Sweden, [6]Present address: National Institute of Neurological Disorders and Stroke, National Institutes of Health, Bethesda, Maryland 20892, [7]These authors contributed equally to this work.

Corresponding author: Olle Lindvall MD PhD

Laboratory of Neurogenesis and Cell Therapy

Wallenberg Neuroscience Center

Lund University Hospital

SE-221 84 Lund

Sweden

Phone: +46-46-222 0543

Fax: +46-46-222 0560

E-mail: olle.lindvall@med.lu.se

Pages (36), Figures (5 + 3 supplementary), Tables (1)

Abstract

We have previously shown that following severe brain insults, chronic inflammation induced by lipopolysaccharide (LPS) injection, and status epilepticus, new dentate granule cells exhibit changes of excitatory and inhibitory synaptic drive indicating that they may mitigate the abnormal brain function. Major inflammatory changes in the environment encountering the new neurons were a common feature of these insults. Here, we have asked how the morphology and electrophysiology of new neurons are affected by a comparably mild pathology: repetitive seizures causing hyperexcitability but not inflammation. Rats were subjected to rapid kindling, i.e., 40 rapidly recurring, electrically-induced seizures, and subsequently exposed to stimulus-evoked seizures twice weekly. New granule cells were labeled 1 week after the initial insult with a retroviral vector encoding green fluorescent protein. After 6-8 weeks, new neurons were analyzed using confocal microscopy and whole-cell patch-clamp recordings. The new neurons exposed to the pathological environment exhibited only subtle changes in their location, orientation, dendritic arborizations, and spine morphology. In contrast to the more severe insults, the new neurons exposed to rapid kindling and stimulus-evoked seizures exhibited enhanced afferent excitatory synaptic drive which could suggest that the cells that had developed in this environment contributed to hyperexcitability. However, the new neurons showed concomitant reduction of intrinsic excitability which may counteract the propagation of this excitability to the target cells. This study provides further evidence that following insults to the adult brain, the pattern of synaptic alterations at afferent inputs to newly generated neurons is dependent on the characteristics of the pathological environment.

Key Words: Adult neurogenesis; seizures; synaptic plasticity; electrophysiology; spines; rat

Introduction

Neural stem/progenitor cells in the adult dentate subgranular zone (SGZ) continuously generate new granule cells (Zhao et al., 2008) which develop functional inputs from the entorhinal cortex (van Praag et al., 2002) and outputs to the hilus and CA3 region (Toni et al., 2008). Synaptic integration of adult-born hippocampal neurons in the intact brain closely resembles that during development (Laplagne et al., 2006) and is conserved throughout life and in old age (Morgenstern et al., 2008). Pathological changes in the stem cell niche and environment encountered by the new neurons influence adult neurogenesis. For example, seizures and cerebral ischemia enhance hippocampal progenitor proliferation and neurogenesis (Bengzon et al., 1997; Parent et al., 1997; Liu et al., 1998) and epileptic insults can lead to aberrant migration of new granule cells (Parent et al., 1997; Parent, 2005). Inflammation is detrimental for the survival of new neurons early after they have been born (Ekdahl et al., 2003; Monje et al., 2003) and pathologies such as Alzheimer's can impair neurogenesis and maturation of new neurons in mice (Biscaro et al., 2009).

How new neurons integrate into existing neural circuitries will determine their action in the diseased brain. Recent experimental evidence indicates that pathological environments influence the morphological and functional integration of adult-born hippocampal neurons. Following kainate-induced status epilepticus (SE) in rats, new granule cells extend abnormal basal dendrites into the hilus and have more mushroom spines on their apical dendrites (Jessberger et al., 2007). We have demonstrated that dentate granule cells born after electrically-

induced SE (eSE) in rats, i.e., into an environment characterized by neuronal death, spontaneous, recurrent seizures and inflammation, exhibit more inhibitory and less excitatory synaptic drive (alterations in frequency and/or amplitude of miniature postsynaptic currents) compared to new neurons from control animals (Jakubs et al., 2006). When exposed to Lipopolysaccharide (LPS)-induced inflammation without seizure activity, new neurons respond with enhanced excitatory and inhibitory drive (Jakubs et al., 2008). Chronic inflammation also gives rise to larger clusters of the postsynaptic GABA receptor scaffolding protein gephyrin on dendrites of new cells (Jakubs et al., 2008). Thus, in pathological environments, adult-born neurons exhibit a high degree of plasticity at their afferent synapses, which may act to mitigate abnormal brain function.

Integration of adult-born neurons has so far been analyzed in pathological environments with pronounced inflammation. How integration is influenced by less severe insults is unknown. The objective of the present study was to determine the morphological and electrophysiological properties of new neurons which developed in a pathological environment with repeated seizures and minimal inflammation. Rats were subjected to an epileptic insult and subsequently exposed to stimulus-evoked seizures twice weekly. New granule cells were labeled 1 week after the initial insult using a retroviral (RV) vector encoding green fluorescent protein (GFP). After 6-8 weeks, new neurons were studied using confocal microscopy and whole-cell patch-clamp recordings. We show that these cells exhibit only minor differences in morphology. Electrophysiological recordings indicate the presence of enhanced afferent excitatory input on the new cells which may be counteracted by reduced membrane excitability. Taken together with our previous studies, these findings indicate that new neurons have mechanisms to counteract or adapt to pathologies at their afferent synaptic inputs, and that the pattern of changes is dependent on the characteristics of the environment.

Material and Methods

Animal groups and rapid kindling. All experimental procedures were approved by the Malmö-Lund Ethical Committee. One-hundred-and-thirty-two male Sprague-Dawley rats were used, weighing 200-250 g at the beginning of the experiments. Animals were anesthetized with isofluorane (1.5-2%) and implanted unilaterally with a bipolar stainless steel stimulating/recording electrode (Plastics One, Roanoke, VA) in the ventral hippocampal CA1-CA3 region (coordinates: 4.8 mm caudal and 5.2 mm lateral to bregma, 6.3 mm ventral from dura, toothbar at -3.3 mm) (Paxinos and Watson, 1997). Another electrode was positioned between the skull and the adjacent muscle to serve as reference. Seven days later, animals were subjected to the rapid kindling protocol (40 stimulations, 1 ms square-wave pulses of 400 μA intensity with 100 Hz intratrain frequency for 10 s every 5 min). For comparisons of the inflammatory response, six rats were subjected to eSE as described previously (Jakubs et al., 2006). The electroencephalogram (EEG) was recorded continuously after stimulation until cessation of focal epileptiform activity (afterdischarge, AD) using Chart 3.6.3 (PowerLab7MacLab, AD Systems). Animals were monitored during this time and behavioral seizures were characterized according to the Racine scale (Racine, 1972). Only animals exhibiting grade 2 seizures and above, and with corresponding ADs were included. Controls were electrode-implanted but not exposed to electrical stimulation.

ELISA. Seven days after rapid kindling or corresponding time point in controls, rats were transcardially perfused with saline and whole hippocampus contralateral to the electrode was rapidly removed and frozen on dry ice. Samples were homogenized on ice in buffer (pH 7.6) containing in (mM): 50.0 Tris-HCl, 150 NaCl, 5.0 $CaCl_2$, 0.02% NaN_3, 1% Triton X-100, and

then centrifuged at 17,000 times gravity for 30 min at +4°C. Protein concentration was determined in supernatants by BCA protein assay (Pierce, USA) and all samples equilibrated to a concentration of 2mg/ml total protein. IL-1β, IL-6, TNF-α, IL-10, and IL-4 concentrations were determined by ELISA (Duoset; R & D Systems, USA) according to manufacturer's instructions. Results are presented as means ± SEM, and statistical comparisons were performed using Student's unpaired t-test. Level of significance was $p < 0.05$.

Labeling of new neurons. Seven days after the rapid kindling procedure, rats were anesthetized with isofluorane and injected with a retrovirus containing the GFP gene (RV-GFP) under the CAG promoter (1.0-1.1 transducing units/ml) (Zhao et al., 2006). Two 1.5 µl retroviral injections were made in the dorsal hippocampus contralateral to the electrode (coordinates: 3.6 mm caudal and 2.0 mm lateral to bregma, and 2.8 mm dorsal to dura; 4.4 mm caudal and 3.0 mm lateral to bregma, and 3.0 mm dorsal to dura; toothbar at -3.3 mm).

Extra stimulations and assessment of excitability. Starting two days after retrovirus injections, animals subjected to rapid kindling were exposed to stimulus-evoked seizures twice weekly for 6-8 weeks. Before and after stimulations, EEG was recorded to determine baseline activity and to observe ADs. Recordings continued until cessation of ADs. Stimulations were delivered for 1 s at AD threshold, as determined by a 1 s 50 Hz electrical current, starting at 10 µA and with 10 µA increments until an AD was registered. At 5 weeks after retrovirus injections, EEG recordings were made on 4 seizure-exposed and 4 non-stimulated control animals for 1 h to assess the occurrence of interictal activity. Mean AD duration (using Chart 3.6.3) and seizure grade were determined for both rapid kindling and extra stimulations. Mean AD threshold was assessed for the extra stimulations. Total AD duration, and mean number and AD duration of partial (grades 1-2) and generalized (grades 4-5) seizures were also calculated

per animal. Development of seizure threshold and seizure grade in response to the consecutive extra stimulations was analyzed using linear regression. Level of significance was $p < 0.05$.

Morphological analysis. At 6-8 weeks after virus injection, animals received an overdose of pentobarbital (250 mg/kg, i.p.) and were transcardially perfused with 100 ml saline and 250 ml 4% paraformaldehyde (PFA) in 0.1M phosphate-buffered saline (PBS), pH 7.4. Brains were cryoprotected in 20% sucrose in 0.1M PBS overnight, cut in 30 µm coronal sections and stored in cryoprotective solution. For characterization of the environment, animals were also perfused and their brains sectioned using the same protocol 1 week after rapid kindling or corresponding time point in controls. For analysis of gephyrin distribution, rats were anesthetized and decapitated, brains were dissected and placed in ice-cold artificial cerebrospinal fluid (aCSF, described below), cut in 300 µm transverse sections and placed in gassed aCSF for 20 min and then in PFA for 10 min (Jakubs et al., 2008). Sections were cryoprotected in 20% sucrose in 0.1M PBS overnight, cut in 12 µm sections and stored at -20^{o}C for at least 1 h.

For immunohistochemistry, the following primary antibodies were used: rabbit anti-Iba1 (1:1000, Wako Chemicals), mouse anti-ED1 (1:200, Serotec), rabbit anti-GFP (1:10000, Abcam), goat anti-IL-1β (1:1000, R&D Systems), and mouse anti-gephyrin (1:10000, Synaptic Systems). Free-floating sections were incubated with the appropriate primary antibody overnight at +4^{o}C and secondary antibody for 1 to 2 h at room temperature. Secondary antibodies were: Cy3-conjugated donkey anti-rabbit (1:200, Jackson ImmunoResearch), biotinylated horse anti-mouse (1:200, Vector Laboratories), biotinylated horse anti-goat (1:200, Vector Laboratories), and FITC-conjugated donkey anti-rabbit (1:200, Jackson ImmunoResearch). Biotinylated antibodies were visualized using Streptavidin-conjugated Alexa Fluor-488 (1:200, Invitrogen). Sections were mounted on gelatin-coated microscope slides and coverslipped. For Fluoro-Jade

staining, mounted sections were pre-treated with 0.06% potassium permanganate before being agitated for 30 min in 0.001% Fluoro-Jade (Histochem) in 0.01% acetic acid, immersed in xylene, and coverslipped with Pertex mounting medium (Histolab).

Cell counting and morphological analysis were performed ipsilaterally to the virus injections in 4 to 6 hippocampal sections by an observer blind to the treatment conditions as previously described (Jakubs et al., 2008). The number of Iba1+, Iba+/ED1+, and Fluoro-Jade+ cells were counted with an Olympus BX61 epifluorescence microscope in the granule cell layer (GCL) and two cell diameters below in the SGZ. Iba1/ED1 double labeling was confirmed by confocal microscopy. The morphological phenotype of Iba1+ cells in the SGZ and GCL was classified into four different subtypes, as previously described (Lehrmann et al., 1997), in 3-4 hippocampal sections. The relative occurrence of each subtype was expressed as the mean percentage of the total number of Iba1+ microglia per section. Stained sections were also examined for double labeling of Iba1+ cells with IL-1β. GFP+ cells were counted in the GCL, SGZ, dentate hilus, and molecular layer (ML). For all GFP+ cells, axon exit point, dendrite exit points, and total number of dendrites leaving the cell soma were analyzed. Dendritic polarity was determined by classifying the angles of the dendrites leaving the cell soma as 0-22^{o}, 22.5-67^{o}, or 67.5-90^{o}, where 90^{o} was perpendicular to the GCL. Location of dendritic branching was determined by assessing the cumulative number of branching points of each dendrite from the cell soma in 15 μm increments. To measure the number of branching points and total dendrite length, a confocal stack was taken of the whole dendritic tree of GFP+ cells in 225 μm thick hippocampal sections. Dendrite length was measured using the NeuronJ plug-in of ImageJ (Meijering et al., 2004).

Spine density (number of spines per micrometer) and morphology (classified as thin, stubby, filopodia, or mushroom spines) (Zhao et al., 2006), and gephyrin cluster density (clusters per micrometer) and size (area in square micrometers) were analyzed by confocal laser scanning microscopy (Bio-Rad MRC1021UV) using Kr-Ar 488 and 568 nm excitation filters with a 63x objective and 16x digital zoom. Analysis was carried out on 12 regions-of-interest (ROI, each 221.4 μm^2) per animal on proximal and distal dendrites in the inner and outer ML, respectively. Cluster area was measured using ImageJ software (Sheffield, 2007).

Results are presented as means ± SEM, and analysis was performed using Student's unpaired t-test or one-way ANOVA with Bonferroni *post-hoc* test for multiple comparisons. Level of significance was $p < 0.05$.

Electrophysiological recordings. 6-8 weeks after virus injections, rats were anesthetized with isofluorane and decapitated. Brains were placed in ice-cold, gassed (95% O_2, 5% CO_2) modified-aCSF (pH 7.2-7.4, 295-300 mOsm), containing (in mM): 225 sucrose, 2.5 KCl, 0.5 $CaCl_2$, 7.0 $MgCl_2$, 28.0 $NaHCO_3$, 1.25 NaH_2PO_4, 7.0 glucose, 1.0 ascorbate, and 3.0 pyruvate. Transverse dorsal hippocampal slices (225 μm), cut on a vibratome (3000 Deluxe, Ted Pella Inc, CA), were placed in an incubation chamber with gassed (95% O_2, 5% CO_2) aCSF (pH 7.2-7.4, 295-300 mOsm) containing (in mM): 119 NaCl, 2.5 KCl, 1.3 $MgSO_4$, 2.5 $CaCl_2$, 26.2 $NaHCO_3$, 1.0 NaH_2PO_4, and 11.0 glucose, and were allowed to rest for at least 1 h at room temperature before recordings.

Individual slices were placed in a submerged recording chamber and perfused with gassed aCSF at +32-34^oC during recordings of miniature excitatory postsynaptic currents (mEPSCs) to optimize event frequency for analysis (Jakubs et al., 2006, 2008), or at room

temperature during recordings of miniature inhibitory postsynaptic currents (mIPSCs) and measurements of intrinsic membrane properties. Cells for recording were visualized using an Olympus upright microscope equipped with a digital camera. GFP-expressing cells were identified under a 40x water immersion lens using fluorescence microscopy. Infrared light with differential interference contrast was used for visual approach and acquiring whole-cell recordings. Recording pipettes with a final tip resistance of 2.5-5.5 MΩ were filled with pipette solution (pH 7.2-7.4, 295-300 mOsm) containing the following (in mM): 122.5 K-gluconate, 12.5 KCl, 10.0 KOH-HEPES, 0.2 KOH-EGTA, 2.0 MgATP, 0.3 Na_3-GTP, and 8.0 NaCl for current-clamp recordings of intrinsic properties; 135.0 CsCl, 10.0 CsOH, 0.2 CsOH-EGTA, 2.0 Mg-ATP, 0.3 Na_3-GTP, 8.0 NaCl and 5.0 lidocaine N-ethyl bromide (QX-314) for voltage-clamp recordings of mIPSCs; or 117.5 Cs-gluconate, 17.5 CsCl, 8.0 NaCl, 10.0 CsOH-HEPES, 0.2 CsOH-EGTA, 2.0 Mg-ATP, 0.3 Na_3-GTP, and 5.0 QX-314 for voltage-clamp recordings of mEPSCs. Biocytin (0.5%, Sigma-Aldrich) was freshly dissolved in the pipette solution before recordings for *post-hoc* identification of recorded cells. Seal resistance was >1 GΩ. For analysis of intrinsic membrane properties, resting membrane potential was estimated in current-clamp mode immediately after breaking the membrane and establishing whole-cell configuration. For measuring current-voltage relationship, 500 ms hyperpolarizing and depolarizing current pulses were delivered in 30 pA increments through the whole-cell pipette. Rheobase was determined by injecting a 300 pA ramp over 1 s. Intrinsic properties were measured in aCSF containing 50 μM D-AP5 and 5 μM NBQX (both Tocris) to block NMDA and non-NMDA receptors, respectively, and 100 μM picrotoxin (PTX) (Tocris) to block $GABA_A$ receptor activation. mIPSCs were recorded in aCSF containing 50 μM D-AP5, 5 μM NBQX, and 1 μM TTX (Tocris) to block action potentials. mEPSCs were recorded with 100 μM PTX and 1 μM TTX in aCSF. To

confirm that recorded cells expressed GFP, fluorescence microscopy was used to detect GFP in the recording pipette, or *post-hoc* immunohistochemical analysis of GFP colocalization with biocytin was conducted.

Data were filtered at 2.9 kHz and sampled at 10 kHz with an EPC9 patch-clamp amplifier (HEKA Elektronik, Lambrecht, Germany). Miniature postsynaptic currents were detected and analyzed using MiniAnalysis software (Synaptosoft). Minimum amplitude for detection was set at 5 times root-mean-square noise level as determined by the software. All detected events were visually controlled. The 10-90% rise time of mEPSCs and mIPSCs were analyzed using MiniAnalysis. Analysis of intrinsic membrane properties was performed using one-way ANOVA with Bonferroni *post-hoc* test for multiple comparisons. Recording duration was 3 minutes and equal numbers of mEPSCs and mIPSCs from each cell were analyzed to prevent any bias. Group interevent intervals (IEIs), amplitudes, and 10-90% rise time were compared using Kolmogorov-Smirnov's statistical test. Mean event frequency was determined from an equal number of events from each cell, and analyzed using Student's unpaired t-test. Level of significance was $p < 0.05$.

Sections from electrophysiology experiments were fixed for 12-24 h in 4% PFA immediately after recordings and stored in antifreeze medium at -20^{o}C. For double staining of biocytin and GFP, free floating sections were preincubated for 1 h in 5% serum in 0.25% Triton X-100 in potassium PBS, and then exposed to rabbit anti-GFP primary antibody (1:10000, Abcam) overnight at room temperature. Immunoreactivity was visualized using FITC-conjugated donkey anti-rabbit secondary antibody and Cy3-streptavadin (both 1:200, Jackson ImmunoResearch). Sections were mounted on glass slides, coverslipped and analyzed using an Olympus BX61 epifluorescence microscope.

Results

Characteristics of the pathological environment

Animals were subjected to rapid kindling (40 supra-threshold stimulations over a period of 3 h and 15 min) followed by twice weekly extra stimulations at AD threshold for 6-8 weeks in order to expose new neurons (labeled with RV-GFP one week after the initial epileptic insult) to repeated seizures but only to mild, or no inflammation during their maturation (Fig. 1A). This protocol was based on our previous data showing that rapid kindling causes AD duration of similar length in the stimulated and non-stimulated hippocampus (Elmer et al., 1998), and on a pilot experiment which indicated that the number of activated microglia (a measure of inflammation) in the dentate gyrus correlated with the number of extra stimulations and generalized seizures and the total AD duration. Using this experimental paradigm, we could address the role of seizures, without introducing major inflammatory changes, on the integration of new neurons. Only animals which showed both behavioral (grade 2 and above) and electroencephalographic seizure activity (Fig. 1B) during rapid kindling and the extra stimulations were included in the study (n = 36). The rapid kindling paradigm produced 23.4 ± 0.4 partial (grade 1-2) and 2.4 ± 0.2 generalized (grade 4-5) seizures per animal, the mean AD duration of partial and generalized seizures was 28.1 ± 3.2 s and 55.7 ± 9.5 s, respectively. The total AD duration per animal during the rapid kindling protocol was 18.5 ± 2 min. The extra stimulations gave rise to 17.5 ± 1.5 partial and 11.8 ± 2.0 generalized seizures and a total AD duration of 9.9 ± 0.9 min per animal. The mean seizure grade progressively increased, and the threshold required to produce an AD gradually decreased (Fig. 1C) with increasing number of extra stimulations, providing evidence for the development of hyperexcitability. However, we observed no pathological interictal activity in the EEG of the seizure-exposed group at 5 weeks

after retrovirus injection or during the extra stimulations, or in the electrode-implanted, non-stimulated group (n = 4 rats/group). These results indicate that the seizure paradigm used here caused development of hyperexcitability in response to stimulations. The occurrences of generalized seizures, in combination with data from previously published studies (Elmer et al., 1998), indicate that the seizure activity spread to both brain hemispheres.

We next assessed in detail the magnitude of inflammation in the seizure-exposed group, first by characterizing the microglial response. At 1 week after rapid kindling, at the time point when the new cells were born (labeled with RV-GFP), there was a modest, non-significant change in the number of activated microglia (Iba1+/ED1+ cells) in the SGZ/GCL (n = 4 rats/group x 4-6 sections/rat, p = 0.06, Fig. 1D-F). Control animals exhibited 13.8 ± 3.5 Iba1+/ED1+ cells/section compared with 34.2 ± 8.3 cells/section 1 week after rapid kindling (148% increase), and 68.1 ± 6.5 cells/section 1 week after eSE (395% increase, n = 6 rats x 4-6 sections/rat), prepared as in our previous study (Jakubs et al., 2006). We then explored whether rapid kindling gave rise to a change in the morphological phenotype of the microglia population. The Iba1+ cells in SGZ/GCL were classified into ramified, intermediate, amoeboid, or round phenotypes using the morphological criteria described by Lehrmann et al. (1997). The severity of a pathological insult determines the degree of microglial activation, round phenotype signifying the most activated state. We observed no change of microglia phenotype at 1 week following rapid kindling (n = 4 rats/group x 3-4 sections/rat, Fig. 1G), arguing against microglia activation. In contrast, when we assessed the morphology of microglia in sections from animals at 1 week after eSE, there was a significant change to a more activated phenotype as compared to control animals, i.e., a decrease of ramified and an increase of intermediate microglia in eSE animals (n = 6 rats x 3-4 sections/rat, *see Supplementary Figure 1*). Taken together, these results provide

evidence that rapid kindling causes a mild pathology without the pronounced microglial activation observed after eSE.

We also assessed the magnitude of hippocampal inflammation at 1 week after rapid kindling by measuring the levels of inflammatory cytokines using ELISA (Fig. 1A). Consistent with our findings that rapid kindling did not cause microglial activation, no significant changes in the levels of IL-1β (control 1188 ± 53 pg/mg; seizures 1254 ± 67 pg/mg), TNF-α (control 146.2 ± 6.5 pg/mg; seizures 156.2 ± 8.7 pg/mg), IL-4 (control 173.7 ± 8.3 pg/mg; seizures 190.2 ± 9.0 pg/mg), IL-6 (control 1928 ± 52 pg/mg; seizures 2002 ± 87 pg/mg), and IL-10 (control 689.6 ± 28.5 pg/mg; seizures 719.6 ± 59.3 pg/mg) were detected in seizure-exposed compared to control animals (n = 8 rats/group). We also did not detect any seizure-induced, increased expression of the pro-inflammatory cytokine IL-1β in Iba1+ microglia in SGZ/GCL using immunohistochemistry (data not shown).

Fluoro-Jade staining revealed no significant neuronal degeneration in the dentate gyrus of the seizure-exposed animals 1 week after rapid kindling stimulations (n = 4 rats/group x 4-6 sections/rat, Fig. 1H, I). Also, we obtained no evidence for chronic inflammation induced by rapid kindling and extra stimulations. Seven weeks after rapid kindling, the number of Iba1+/ED1+ cells did not differ between seizure-exposed and control animals (n = 4 rats/group x 4-6 sections/rat, Fig. 1F). Taken together, our findings show that the new neurons generated 1 week after rapid kindling developed in an environment characterized by repeated seizures and gradual development of hyperexcitability but without significant neuronal death or inflammation.

Morphological integration of the new neurons in the pathological environment

Six to eight weeks after virus injection, stable GFP expression was observed in a substantial number of new dentate granule cells in non-stimulated, electrode-implanted controls and seizure-exposed animals (Fig. 2A, B). In accordance with previous studies reporting that seizures enhance neural/stem progenitor cell proliferation (Bengzon et al., 1997; Parent et al., 1997; Scott et al., 1998), there were noticeably more new GFP+ cells in seizure-exposed animals compared to control animals. The distribution of the new cells within the GCL did not differ between seizure-exposed and non-stimulated animals, the majority being located within the inner GCL (n = 8 control rats, 5 seizure-exposed rats x 4-6 sections/rat, Fig. 2C). Very few aberrant neurons were observed in the hilus in both groups. The total number of dendrites per new cell (control 1.3 ± 0.07; seizures 1.1 ± 0.08), and the polarity of dendrites leaving the cell soma did not differ between the groups, most of the dendrites leaving at a 67.5-90^{o} angle in relation to the GCL (control 72.0 ± 7.1%; seizures 56.7 ± 3.7%) (n = 7 control rats, 6 seizure-exposed rats x 4-6 sections/rat). Dendrite development was similar in seizure-exposed and control new cells, as no differences were detected in, (*i*) dendrite length (control 1.87 ± 0.15 mm; seizures 1.95 ± 0.16 mm; $p > 0.05$), (*ii*) dendrite exit point from cell soma or number of recurrent basal dendrites (Fig. 2D), or (*iii*) number of branching points (control 8.3 ± 1.15 points/cell; seizures 6.3 ± 0.49 points/cell; $p > 0.05$) or location of dendrite branches (Fig. 2E). Axons primarily originated from the basal (control 80.0%; seizures 79.2%) and medial soma (control 16.0%; seizures 18.8%) and rarely from the apical side (control 4.0%; seizures 2.0%). These results indicate that the pathological environment caused by rapid kindling and repeated extra stimulations did not interfere with the gross morphological appearance of the new neurons.

We next investigated whether the pathological environment affected the morphological development of the synaptic inputs on the new granule cells. Using confocal microscopy and

ImageJ we did not detect any difference in the total spine density in the inner or outer ML between the seizure-exposed and non-stimulated group (n = 8 rats/group x 12 ROI/rat, Fig. 2F).We next examined the individual spine subtypes based on their morphology. Filopodia and stubby spines are considered immature spine phenotypes whereas thin and mushroom spines are regarded as more mature (Nimchinsky et al., 2002). There was no difference in the density of thin and mushroom spines or in filopodia between the two groups. However, the seizure-exposed group had significantly more stubby spines than the non-stimulated group (Fig. 2F), indicating that this pathological environment induced subtle alterations of excitatory synapses. We have previously reported that chronic inflammation causes increased size of gephyrin clusters on the dendrites of new dentate granule cells (Jakubs et al., 2008). Gephyrin is a scaffolding protein associated with clustering of glycine and $GABA_A$ receptors at inhibitory synapses (Fritschy et al., 2008). Here we found that the density of gephyrin clusters on the dendrites of the new cells was similar in control and seizure-exposed animals (0.16 ± 0.03 cluster/μm and 0.20 ± 0.02 cluster/μm, respectively, $p > 0.05$, n = 5 rats/group x 12 ROI/rat) (Fig. 2G, H). Furthermore, the gephyrin cluster size did not differ between the groups (control 0.19 ± 0.01 μm^2; seizures 0.19 ± 0.01 μm^2, $p > 0.05$).

Functional integration of the new neurons in the pathological environment

Whole-cell patch-clamp recordings were performed from GFP+ cells (new cells, born at the time of RV-GFP injection) and neighboring GFP- cells (mature cells, most likely born before the onset of recurrent seizures) (Jakubs et al., 2006) in the GCL at 6-8 weeks after the RV-GFP injection. Mature, GFP- cells were selected based on their position within the GCL and their

morphology. Immunohistochemistry performed after recordings revealed development of mature dendrites on both GFP- and GFP+ neurons. We found that the intrinsic membrane properties (resting membrane potential, input resistance, series resistance, action potential threshold, and action potential half-width) of the new and mature cells in seizure-exposed animals were not significantly different compared to new and mature cells in non-stimulated, electrode-implanted controls (Table 1, Fig. 3A, B). These properties were also similar to those characteristic of dentate granule cells (Staley et al., 1992). A recent study reported that rheobase (amount of current required to depolarize membrane potential to threshold level for action potential generation) was increased in granule cells in a model of temporal lobe epilepsy (Young et al., 2009). Interestingly, we detected an increase in rheobase in the seizure-exposed new cells compared to all other groups. Furthermore, ramp current injection elicited fewer action potentials in seizure-exposed compared to control new cells (control 5.6 ± 0.7, $n = 7$ cells from 5 rats; seizures 3.4 ± 0.5, $n = 8$ cells from 4 rats; $p < 0.05$, Fig 3C).

We then explored whether the environment created by the initial epileptic insult and the repeated seizures influenced the network-independent excitatory and inhibitory synaptic input to the new neurons in the GCL (*for recordings of mEPSCs and mIPSCs in mature cells, see Supplementary Figure 2-3*). Whole-cell voltage-clamp recordings of mEPSCs were carried out in the presence of the $GABA_A$ receptor antagonist PTX and voltage-gated sodium channel blocker TTX. Cumulative fraction analysis showed that the new cells which were exposed to seizures throughout development exhibited mEPSCs of larger amplitude compared to new cells from control animals (Fig 4A, E). Moreover, new cells exposed to seizures exhibited mEPSCs with faster rise times compared to control new cells (Fig. 4B). Both these changes in mEPSCs are considered to be indicative of postsynaptic alterations. The mean frequency of mEPSCs tended

to be higher in new cells exposed to seizures but this difference did not reach statistical significance, possibly due to the low number of cells accessible for recording (Fig. 4C). Since histograms of IEIs were skewed, indicating non-normal distribution (data not shown), non-parametric, cumulative fraction analysis was applied. This analysis revealed shorter IEIs of mEPSCs in new seizure-exposed cells compared to new cells from control animals (Fig. 4D), providing evidence for an increase in mEPSC frequency. Thus, our results indicate that adult-born granule cells, exposed to repeated seizures throughout development, receive enhanced excitatory drive, which is independent of network-generated action potentials.

We also determined if the new neurons exhibited altered inhibitory synaptic input when born after rapidly recurring seizures and subsequently exposed to episodes of seizure activity throughout their development. Whole-cell voltage-clamp recordings of mIPSCs were performed while blocking glutamate receptors with NBQX and D-AP5, and action potentials with TTX. Cumulative fraction analysis showed that the amplitude of mIPSCs was not different between new cells born into the seizure environment and new cells from control animals (Fig. 5A, E). However, mIPSCs from seizure-exposed new cells exhibited slower 10-90% rise times compared to control new cells (Fig. 5B), suggesting a relative decrease in the strength of perisomatic vs. dendritic inhibitory drive (Kobayashi and Buckmaster 2003; Jakubs et al., 2006; however, see Soltesz et al., 1995). We next looked at the frequency and IEIs of mIPSCs. mIPSCs occurred with lower mean frequency in seizure-exposed as compared to control new cells, but the difference was not statistically significant (Fig. 5C). However, when we used cumulative fraction analysis due to the skewed, non-normal distribution of IEIs, we detected lengthening of mIPSC IEIs in seizure-exposed compared to control new cells (Fig. 5D), suggesting a decrease in mIPSC frequency. Taken together, our results indicate that, in the absence of network-generated action

potentials, adult-born granule cells exposed to repeated seizures throughout their development receive reduced perisomatic inhibition compared to new cells born in control animals.

Discussion

How neurons, which are born and develop in a pathological environment, integrate into existing neural circuitries in the adult brain will determine whether they counteract or contribute to functional impairments. Here we show that new dentate granule cells generated following an epileptic insult, comprising 40 rapidly recurring seizures, and exposed to repeated seizures during their differentiation exhibited increased overall synaptic excitability compared to new cells which had developed in a normal environment. The increased synaptic excitability of these cells may be counterbalanced, or even overridden by reduced intrinsic excitability as evidenced by higher rheobase. In contrast, detailed morphological analysis of the location, orientation, dendritic arborizations, and spines of these cells showed only minor differences between the groups.

Our finding that new granule cells received enhanced excitatory drive after seizures is consistent with studies which have reported enhanced excitability of dentate granule cells after pilocarpine-induced seizures (Simmons et al., 1997) and kainate-induced seizures (Wuarin and Dudek, 2001). How seizures influence the inhibition of granule cells is less clear as there are reports that kainate-induced seizures enhance (Buckmaster and Dudek, 1997) whereas pilocarpine-induced seizures reduce inhibitory input to granule cells (Kobayashi and Buckmaster, 2003). Furthermore, after eSE, mature granule cells exhibit longer IEIs of sIPSCs with larger amplitude (Jakubs et al., 2006). Inhibition may be influenced by changes in zinc

distribution. After kindling, granule cells receive increased inhibitory drive, which may collapse due to zinc released from aberrantly sprouted mossy fibers interacting with zinc-sensitive $GABA_A$ receptors (Buhl et al., 1996). We found that new granule cells born after rapid kindling and exposed to repeated seizures exhibited mIPSCs of similar amplitude but with longer IEIs compared to new cells in control animals. Taken together, it seems that changes in the inhibitory inputs to granule cells are dependent on the seizure paradigm and epilepsy model used, and may be modulated at both pre- and postsynaptic sites.

Two main lines of evidence indicate that the new neurons born after rapid kindling and exposed to repeated seizures integrate into hippocampal circuitry in a manner that may contribute to enhanced synaptic excitability. First, mEPSCs in seizure-exposed new cells had larger amplitudes and faster rise times compared to mEPSCs recorded in control new cells. These changes, including excitatory postsynaptic receptor kinetics, are consistent with alterations of AMPA receptor subunits (Koike et al., 2000; Liu and Cull-Candy, 2000). Second, mIPSCs in seizure-exposed new cells display longer rise times of mIPSCs, which suggest a relative weakening of perisomatic inhibition in seizure-exposed new cells (Kobayashi and Buckmaster 2003; Jakubs et al., 2006; however, see Soltesz et al., 1995). If this is the case, it could lead to less control over action potentials thought to be generated around the axon hillock, i.e., in the perisomatic area. These changes in postsynaptic receptor kinetics may also indicate changes in $GABA_A$ receptor subunits (Coulter, 2001). However, in the same seizure-exposed new cells, we also observed increased rheobase and fewer action potentials, which may partially, or completely, counteract the enhanced synaptic excitability.

The exact source of the presynaptic input to the new neurons and their postsynaptic targets remain important issues. It is well established that the entorhinal cortex via the perforant

path is the primary source of excitatory input to mature dentate granule cells and also adult-born neurons (Overstreet-Wadiche et al., 2006). However, there is evidence that after seizures, granule cells can provide excitatory input to each other due to mossy fiber sprouting (Tauck and Nadler, 1985; Elmér et al., 1996; Sutula et al., 1989; Represa et al., 1990). Inhibitory interneurons located throughout the hippocampus provide GABAergic input to granule cells. The number of interneurons, their morphology, and development of synapses with granule cells is influenced by seizures (Wittner et al., 2001; Dinocourt et al., 2003; Sayin et al., 2003; Zhang and Buckmaster, 2009). To what extent mossy fiber sprouting or alterations of inhibitory interneurons influence the integration of the new neurons is not known.

The pre- and postsynaptic changes observed here indicate a net increase in the excitatory drive onto the seizure-exposed new neurons, but how this influences their functional output is unclear. Axons of dentate granule cells (mossy fibers) contact hilar mossy cells, CA3 pyramidal cells and hilar interneurons. Enhanced rheobase may prevent the cells from propagating this excitability to the targets of their efferent synapses. The changes in rheobase likely indicate alterations in the membrane properties of the seizure-exposed cells, particularly changes in the input resistance of the cell (Young et al., 2009). We found that the input resistance of the seizure-exposed new cells tended to be lower compared to that of the other recorded cells (although not statistically significant), which may partially explain the increase in rheobase. Changes in input resistance suggest alterations in the number, distribution, or composition of membrane channels in the new cells. It should be emphasized, finally, that the functional significance at the network level of the altered afferent synaptic inputs to the new cells, whether they will counteract or contribute to the development of hyperexcitability, will depend on the synaptic influence of these

cells on their target neurons (Frotscher et al., 2006), an issue that is highly warranted to address in future studies.

The pattern of alterations in afferent excitatory and inhibitory synaptic drive on the new cells in the present seizure paradigm differs from that we have previously reported following eSE (Jakubs et al., 2006). In response to the eSE insult, the new neurons exhibited reduced excitatory and increased inhibitory synaptic drive (Jakubs et al., 2006). The eSE insult comprised approximately 3 h of seizure activity and the environment surrounding the new cells was characterized by neuronal death, chronic inflammation and spontaneous seizures. In contrast, we observed here no significant inflammatory changes or neuronal death in the pathological environment. The total duration of seizures induced by the rapid kindling protocol was much shorter (about 19 min). The eSE environment was associated with abnormal excitability, as evidenced by spontaneous behavioral seizures, whereas following rapid kindling, there was a progressive development of hyperexcitability but no interictal spikes or spontaneous seizures were detected. The stimulus-evoked seizures lasted for in total about 10 min. Taken together, the discrepancy in afferent synaptic connectivity, comparing the present findings with our previous data (Jakubs et al., 2006), indicates that the integration of the new cells depends on the type of pathological environment they encounter.

The characteristics of the pathological environment will also determine its influences on the morphological development of the new neurons. Walter et al. (2007) studied new granule cells exposed to 3 h of pilocarpine-induced SE in mice either at 1 week after they had been generated or when they were born into the pathological environment 3 weeks after the insult. This insult, which caused spontaneous seizures and extensive neuronal death in the dentate hilus and variable cell loss in CA1 and CA3 regions, gave rise to the formation of basal dendrites

projecting into the hilus in 40-50% of new granule cells. Such dendrites are virtually absent in intact animals. Also, Jessberger et al. (2007) found basal hilar dendrites in about 20% of new granule cells born at 1 week following 2-3 h of kainate-induced SE. It is conceivable that both these severe epileptic insults were associated with inflammation. In contrast, the present epileptic insult, in which the total duration of seizure activity was much shorter, resulted in no significant inflammation or neuronal death, and the occurrence of very few basal hilar dendrites on the new granule cells. Our findings, that new neurons which develop in the presence of seizures without inflammation exhibit no major morphological changes indicate that the occurrence of morphological abnormalities is likely dependent on the severity of pathology in the environment.

We found an increased number of stubby spines on the seizure-exposed new cells. Stubby spines have been found to be more frequent on mature hippocampal dendrites in acute slices with blocked synaptic transmission, which is believed to recapitulate development (Petrak et al., 2005). Interestingly, application of brain-derived neurotrophic factor (BDNF) to hippocampal slice cultures under serum-free conditions specifically promoted the formation of stubby spines on mature CA1 pyramidal neurons (Tyler and Pozza-Miller, 2003, however, see Chapleau et al., 2008). These stubby spines may have a role in Ca^{2+}-dependent synaptic plasticity (Tyler and Pozzo-Miller, 2003). BDNF has also been proposed to be an important regulator of morphological and functional hippocampal plasticity in response to seizures (Ernfors et al., 1991; Kokaia et al., 1995; Binder et al., 2001). Hypothetically, BDNF signaling may have contributed to the increase of stubby spines observed here on the new cells.

Inflammation regulates several steps of adult neurogenesis including survival, proliferation, migration, differentiation, and functional integration of the new neurons (reviewed by Ekdahl et al., 2009). LPS-induced chronic inflammation gave rise to a similar increase of

excitatory synaptic drive in new and mature dentate granule cells, probably due to increased network activity (Jakubs et al., 2008). Also, inhibitory synaptic drive was increased by inflammation in both new and mature cells but more enhanced in the new cells. In line with this observation, larger clusters of the postsynaptic $GABA_A$ receptor scaffolding protein gephyrin were found on dendrites of new cells born in the inflammatory environment. It is conceivable that the larger gephyrin clusters indicate a more efficacious inhibitory input and contributes to the synapse-specific enhancement of the afferent inhibitory drive. In contrast, we found here that the new cells which had been born after rapid kindling and exposed to repeated seizures did not exhibit any change in mIPSC amplitude, indicating no postsynaptic alterations. In accordance, we did not observe any alteration in the density or size of gephyrin clusters at postsynaptic sites in neurons which had developed in this environment. The present findings provide further evidence for an important regulatory role of inflammation for inhibitory synaptic drive on the new cells. Our data indicate that different pathological environments, associated with varying magnitude of inflammation, differ with respect to their ability to induce postsynaptic changes in new cells which will influence the efficacy of their afferent inputs.

The present findings show that adult-born, new neurons exhibit a high degree of plasticity at their afferent synapses when developing in a pathological environment. Our previous data following eSE (Jakubs et al., 2006) and chronic inflammation (Jakubs et al., 2008) suggested that the functional integration of the new neurons may act to mitigate the pathological condition. Here, the new neurons responded to repeated seizures in an environment without inflammation by overall more synaptic excitability, which may be counteracted by the reduced intrinsic excitability compared to control new cells. If this is the case, the new neurons may have a limited contribution to the hyperexcitability which develops during the course of their maturation or

even counteract the abnormal function. In conclusion, our findings indicate that the characteristics of the pathological environment, e.g., the magnitude of inflammation and the seizure paradigm, will play an important role in determining whether the new neurons will counteract or contribute to abnormal brain function.

Acknowledgements

This work was supported by the Swedish Research Council, Juvenile Diabetes Research Foundation, and EU project LSHB-2006-037526 (StemStroke). We thank Dr. Fred H. Gage and Dr. H. van Praag for RV-GFP, and Dr. Sara Bonde and Dr. Robert E. Iosif for preparation of animals during the initial part of the study.

References

Bengzon, J., Kokaia, Z., Elmer, E., Nanobashvili, A., Kokaia, M., Lindvall, O., 1997. Apoptosis and proliferation of dentate gyrus neurons after single and intermittent limbic seizures. Proc Natl Acad Sci U S A. 94, 10432-10437.

Binder, D.K., Croll, S.D., Gall, C.M., Scharfman, H.E., 2001. BDNF and epilepsy: too much of a good thing? Trends Neurosci. 24, 47-53.

Biscaro, B., Lindvall, O., Hock, C., Ekdahl, C.T., Nitsch, R.M., 2009. Abeta immunotherapy protects morphology and survival of adult-born neurons in doubly transgenic APP/PS1 mice. J Neurosci. 29, 14108-14119.

Buckmaster, P.S., Dudek, F.E., 1997. Neuron loss, granule cell axon reorganization, and functional changes in the dentate gyrus of epileptic kainate-treated rats. J Comp Neurol. 385, 385-404.

Buhl, E.H., Otis, T.S., Mody, I., 1996. Zinc-induced collapse of augmented inhibition by GABA in a temporal lobe epilepsy model. Science. 271, 369-373.

Chapleau, C.A., Carlo, M.E., Larimore, J.L., Pozzo-Miller, L., 2008. The actions of BDNF on dendritic spine density and morphology in organotypic slice cultures depend on the presence of serum in culture media. J Neurosci Methods. 169, 182-190.

Coulter, D.A., 2001. Epilepsy-associated plasticity in gamma-aminobutyric acid receptor expression, function, and inhibitory synaptic properties. Int Rev Neurobiol. 45, 237-52. Review.

Dinocourt, C., Petanjek, Z., Freund, T.F., Ben-Ari, Y., Esclapez, M., 2003. Loss of interneurons innervating pyramidal cell dendrites and axon initial segments in the CA1 region of the hippocampus following pilocarpine-induced seizures. J Comp Neurol. 459, 407-425.

Ekdahl, C.T., Kokaia, Z., Lindvall, O., 2009. Brain inflammation and adult neurogenesis: the dual role of microglia. Neuroscience. 158, 1021-1029.

Ekdahl, C.T., Claasen, J.H., Bonde, S., Kokaia, Z., Lindvall, O., 2003. Inflammation is detrimental for neurogenesis in adult brain. Proc Natl Acad Sci U S A. 100, 13632-13637.

Elmér, E., Kokaia, M., Kokaia, Z., Ferencz, I., Lindvall, O., 1996. Delayed kindling development after rapidly recurring seizures: relation to mossy fiber sprouting and neurotrophin, GAP-43 and dynorphin gene expression. Brain Res. 712, 19-34.

Elmér, E., Kokaia, Z., Kokaia, M., Carnahan, J., Nawa, H., Lindvall, O., 1998. Dynamic changes of brain-derived neurotrophic factor protein levels in the rat forebrain after single and recurring kindling-induced seizures. Neuroscience. 83, 351-362.

Ernfors, P., Bengzon, J., Kokaia, Z., Persson, H., Lindvall, O., 1991. Increased levels of messenger RNAs for neurotrophic factors in the brain during kindling epileptogenesis. Neuron. 7, 165-176.

Fritschy, J.M., Harvey, R.J., Schwarz, G., 2008. Gephyrin: where do we stand, where do we go? Trends Neurosci. 31,257-264.

Frotscher, M., Jonas, P., Sloviter, R.S., 2006. Synapses formed by normal and abnormal hippocampal mossy fibers. Cell Tissue Res. 326, :361-367.

Jakubs, K., Nanobashvili, A., Bonde, S., Ekdahl, C.T., Kokaia, Z., Kokaia, M., Lindvall, O., 2006. Environment matters: synaptic properties of neurons born in the epileptic adult brain develop to reduce excitability. Neuron. 52, 1047-1059.

Jakubs, K., Bonde, S., Iosif, R.E., Ekdahl, C.T., Kokaia, Z., Kokaia, M., Lindvall, O., 2008. Inflammation regulates functional integration of neurons born in adult brain. J Neurosci. 28, 12477-12488.

Jessberger, S., Zhao, C., Toni, N., Clemenson, G.D. Jr., Li, Y., Gage, F.H., 2007. Seizure-associated, aberrant neurogenesis in adult rats characterized with retrovirus-mediated cell labeling. J Neurosci. 27, 9400-9407.

Kobayashi, M., Buckmaster, P.S., 2003. Reduced inhibition of dentate granule cells in a model of temporal lobe epilepsy. J Neurosci. 23, 2440-2452.

Koike, M., Tsukada, S., Tsuzuki, K., Kijima, H., Ozawa, S., 2000. Regulation of kinetic properties of GluR2 AMPA receptor channels by alternative splicing. J Neurosci. 20, 2166-74.

Kokaia, M., Ernfors, P., Kokaia, Z., Elmer, E., Jaenisch, R., Lindvall, O., 1995. Suppressed epileptogenesis in BDNF mutant mice. Exp Neurol. 133, 215-224.

Laplagne, D.A., Esposito, M.S., Piatti, V.C., Morgenstern, N.A., Zhao, C., van Praag, H., Gage, F.H., Schinder, A.F., 2006. Functional convergence of neurons generated in the developing and adult hippocampus. PLoS Biol. 4, e409.

Lehrmann, E., Christensen, T., Zimmer, J., Diemer, N.H., Finsen, B. 1997. Microglial and macrophage reactions mark progressive changes and define the penumbra in the rat neocortex and striatum after transient middle cerebral artery occlusion. J Comp Neurol. 386, 461-76.

Liu, J., Solway, K., Messing, R.O., Sharp, F.R., 1998. Increased neurogenesis in the dentate gyrus after transient global ischemia in gerbils. J Neurosci. 18, 7768-7778.

Liu, S.Q., Cull-Candy, S.G., 2000. Synaptic activity at calcium-permeable AMPA receptors induces a switch in receptor subtype. Nature. 405, 454-8.

Meijering, E., Jacob, M., Sarria, J.C.F., Steiner, P., Hirling, H., Unser, M., 2004. Design and validation of a tool for neurite tracing and analysis in fluorescence microscopy images. Cytometry. 2, 167-176.

Monje, M.L., Toda, H., Palmer, T.D., 2003. Inflammatory blockade restores adult hippocampal neurogenesis. Science. 302, 1760-1765.

Morgenstern, N.A., Lombardi, G., Schinder, A.F., 2008. Newborn granule cells in the ageing dentate gyrus. J Physiol. 586, 3751-3757.

Nimchinsky, E.A., Sabatini, B.L., Svoboda, K., 2002. Structure and function of dendritic spines. Annu Rev Physiol. 64, 313-353.

Overstreet-Wadiche, L.S., Bromberg, D.A., Bensen, A.L., Westbrook, G.L, 2006 Seizures accelerate functional integration of adult-generated granule cells. J Neurosci. 26, 4095-4103.
Parent, J.M., 2005. When newborn neurons stray. Epilepsy Curr. 5, 231-233.

Parent, J.M., Yu, T.W., Leibowitz, R.T., Geschwind, D.H., Sloviter, R.S., Lowenstein, D.H., 1997. Dentate granule cell neurogenesis is increased by seizures and contributes to aberrant network reorganization in the adult rat hippocampus. J Neurosci. 17, 3727-3738.

Paxinos, G., Watson, C., 1997. The Rat Brain in Stereotaxic Coordinates. San Diego, Academic.

Petrak, L.J., Harris, K.M., Kirov, S.A., 2005. Synaptogenesis on mature hippocampal dendrites occurs via filopodia and immature spines during blocked synaptic transmission. J Comp Neurol. 484, 183-190.

Racine, R.J., 1972. Modification of Seizure Activity by Electrical Stimulation. II. Motor Seizure. Electroencephalogr Clin Neurophysiol. 32, 281-294.

Represa, A., Tremblay, E., Ben-Ari, Y., 1990. Sprouting of mossy fibers in the hippocampus of epileptic human and rat. Adv Exp Med Biol. 268, 419-424.

Sayin, U., Osting, S., Hagen, J., Rutecki, P., Sutula, T., 2003. Spontaneous seizures and loss of axo-axonic and axo-somatic inhibition induced by repeated brief seizures in kindled rats. J Neurosci. 23, 2759-2768.

Scott, B.W., Wang, S., Burnham, W.M., De Boni, U., Wojtowicz, J.M., 1998. Kindling-induced neurogenesis in the dentate gyrus of the rat. Neurosci Lett. 248, 73-76.

Sheffield, J.B., 2007. ImageJ, a useful tool for biological image processing and analysis. Microsc Microanal. 13, 200-201.

Simmons, M.L., Terman, G.W., Chavkin, C., 1997. Spontaneous excitatory currents and kappa-opioid receptor inhibition in dentate gyrus are increased in the rat pilocarpine model of temporal lobe epilepsy. J Neurophysiol. 78, 1860-1868.

Soltesz, I., Smetters, D.K., Mody, I., 1995. Tonic inhibition originates from synapses close to the soma. Neuron. 14, 1273-1283.

Staley, K.J., Otis, T.S., Mody, I., 1992. Membrane-Properties of Dentate Gyrus Granule Cells - Comparison of Sharp Microelectrode and Whole-Cell Recordings. J Neurophysiol. 67, 1346-1358.

Sutula, T., Cascino, G., Cavazos, J., Parada, I., Ramirez, L., 1989. Mossy fiber synaptic reorganization in the epileptic human temporal lobe. Ann Neurol. 26, 321-330.

Tauck, D.L., Nadler, J.V., 1985. Evidence of functional mossy fiber sprouting in hippocampal formation of kainic acid-treated rats. J Neurosci. 5, 1016–1022.

Toni, N., Laplagne, D.A., Zhao, C., Lombardi, G., Ribak, C.E., Gage, F.H., Schinder, A.F., 2008. Neurons born in the adult dentate gyrus form functional synapses with target cells. Nat Neurosci. 11, 901-907.

Tyler, W.J., Pozzo-Miller, L., 2003. Miniature synaptic transmission and BDNF modulate dendritic spine growth and form in rat CA1 neurones. J Physiol-London. 553, 497-509.

van Praag, H., Schinder, A.F., Christie, B.R., Toni, N., Palmer, T.D., Gage, F.H., 2002. Functional neurogenesis in the adult hippocampus. Nature. 415, 1030-1034.

Walter, C., Murphy, B.L., Pun, R.Y.K., Spieles-Engemann, A.L., Danzer, S.C., 2007. Pilocarpine-induced seizures cause selective time-dependent changes to adult-generated hippocampal dentate granule cells. J Neurosci. 27, 7541-7552.

Wittner, L., Maglóczky, Z., Borhegyi, Z., Halász, P., Tóth, S., Eross, L., Szabó, Z., Freund, T.F., 2001. Preservation of perisomatic inhibitory input of granule cells in the epileptic human dentate gyrus. Neuroscience. 108, 587-600.

Wuarin, J.P., Dudek, F.E., 2001. Excitatory synaptic input to granule cells increases with time after kainate treatment. J Neurophysiol. 85, 1067-1077.

Young, C.C., Stegen, M., Bernard, R., Müller, M., Bischofberger, J., Veh, R.W., Haas, C.A., Wolfart, J., 2009. Upregulation of inward rectifier K+ (Kir2) channels in dentate gyrus granule cells in temporal lobe epilepsy. J Physiol. 587, 4213-33.

Zhang, W., Buckmaster, P.S., 2009. Dysfunction of the dentate basket cell circuit in a rat model of temporal lobe epilepsy. J Neurosci. 29, 7846-7856.

Zhao, C.M., Teng, E.M., Summers, R.G., Ming, G.L., Gage, F.H., 2006. Distinct morphological stages of dentate granule neuron maturation in the adult mouse hippocampus. J Neurosci. 26, 3-11.

Zhao, C.M., Deng, W., Gage, F.H., 2008. Mechanisms and functional implications of adult neurogenesis. Cell. 132, 645-660.

Table Legends

Table 1. Recordings were made from new (GFP+) and mature (GFP-) cells in animals subjected to rapid kindling and repeated seizures or non-stimulated control animals at 6-8 weeks after RV-GFP injection. Means ± SEM. Comparisons using one-way ANOVA with Bonferroni *post-hoc* test revealed no significant differences ($p > 0.05$) except for rheobase. *Significantly higher compared to all other groups ($p < 0.05$). Number of recorded cells: new cells-seizures: 8 cells from 4 rats, new cells-control: 7 cells from 5 rats, mature cells-seizures: 8 cells from 7 rats, mature cells-control: 9 cells from 6 rats.

Table 1. Intrinsic Membrane Properties of GFP+ and GFP- cells in the Dentate Granule Cell Layer

	Control GFP+	Control GFP-	Seizures GFP+	Seizures GFP-
Resting membrane potential (mV)	-79.0 ± 2.1	-80.3 ± 1.4	-80.3 ± 1.1	-81.3 ± 1.4
Input Resistance (MΩ)	321 ± 24.5	355 ± 58.9	281 ± 28.9	415 ± 34.1
Series Resistance (MΩ)	13.3 ± 2.3	10.1 ± 1.1	12.3 ± 1.1	14.4 ± 1.5
Action potential Threshold (mV)	-47.8 ± 2.1	-48.9 ± 2.5	-43.9 ± 1.3	-48.1 ± 1.6
Action potential half-width (ms)	1.26 ± 0.09	1.23 ± 0.05	1.42 ± 0.06	1.22 ± 0.05
Rheobase (pA)	131 ± 9	136 ± 19	194 ± 11*	94 ± 8

Figure Legends

Figure 1. Pathological environment is characterized by repeated seizures and no significant inflammation. *A,* Schematic representation of experimental timeline. *B*, EEG recordings from electrode-implanted animals showing baseline activity (top) before stimulations, high-frequency ictal activity following stimulation during the rapid kindling protocol (middle), and high-frequency ictal activity following an extra stimulation (bottom). Scale bar is 2 s, 1 mV. C_1, Increased seizure grade and (C_2) decreased seizure threshold in response to the extra stimulations (Means ± SEM, linear regression). Iba+ (green), ED1+ (red), and Iba1+/ED1+ (yellow, arrowheads, inset) cells 1 week after rapid kindling in control (*D*) and seizure-exposed (*E*) animals (h, hilus; GCL, granule cell layer). *F*, Minimal increase of activated microglia (Iba1+/ED1+ cells) 1 week after rapid kindling and no difference compared to control at 7 weeks. *G*, No differences between seizure-exposed and control animals in morphological phenotype of Iba1+ microglia. Lack of Fluoro-Jade-stained degenerating neurons in control animals 2 weeks after electrode implantation (*H*) and in seizure-exposed animals 1 week after rapid kindling (*I*). Scale bars = 10 μm. Means ± SEM.

Figure 2. New neurons exposed to repeated seizures without inflammation exhibit minor morphological changes. GFP+ cell bodies in the GCL with dendrites extending into the ML and axons into the hilus (*h*) 6 weeks after virus injection in control (*A*) and seizure-exposed (*B*) animals. Insets show representative images of GFP+ new cells. *C*, Relative location of GFP+ cells in inner, middle, or outer GCL (iGCL, mGCL, and oGCL, respectively), or hilus. *D*, Relative occurrence of apical, basal, or recurrent basal dendrites (RBD) on GFP+ cells. *E*,

Cumulative number of dendritic branching points at increasing distances from the GFP+ cell body. *F*, Spine density on GFP+ dendrites from seizure-exposed and control animals (*, increased density on seizure-exposed compared to control new cells, Student's unpaired t-test, $p < 0.05$). Representative images of gephyrin clusters (arrows) in control (*G*) and seizure-exposed (*H*) animals. Scale bars = 50 μm (in A, B) and 1μm (in G, H). Means ± SEM.

Figure 3. New neurons exposed to repeated seizures without inflammation have similar intrinsic membrane properties but reduced intrinsic excitability compared to new neurons in control environment. *A*, Representative traces of action potentials elicited in a control new cell and a seizure-exposed new cell. Scale bar = 100 ms, 20 mV. *B*, Voltage responses in control and seizure-exposed new cells. *C*, Representative traces of membrane potential responding to ramp current injection showing increased rheobase and fewer action potentials in seizure-exposed new cells. Scale bar = 500 ms, 20 mV. Representative traces.

Figure 4. New neurons exposed to repeated seizures without inflammation exhibit enhanced excitatory input in the absence of network activity. Cumulative fraction curve showing increased amplitude and faster 10-90% rise time of mEPSCs in new cells from seizure-exposed compared to new cells from control animals after action potential blockade with TTX (*A, B*). No change in mean event frequency (Student's unpaired t-test, $p > 0.05$), but shorter IEI of mEPSCs in new cells exposed to seizures compared to control new cells (*C, D*) (Kolmogorov-Smirnov test). *E*, Representative traces of mEPSCs in seizure-exposed and control cells. 1, 2 depict representative events (*left*) on an expanded time scale (*right*). Scale bar = 10 pA, 1 s and 10 pA, 5 ms,

respectively. Number of recorded cells: new cells-seizures: 6 cells from 4 rats, new cells-control: 8 cells from 5 rats.

Figure 5. New neurons exposed to repeated seizures without inflammation exhibit altered inhibitory input in the absence of network activity. Cumulative fraction curves showing no change in amplitude and slower 10-90% rise time of mIPSCs in new cells from seizure-exposed compared to control animals after action potential blockade with TTX (*A, B*). No change in mean event frequency (Student's unpaired t-test, $p > 0.05$), but longer IEI of mIPSCs in new cells exposed to seizures compared to control new cells (*C, D*). (Kolmogorov-Smirnov test). *E*, Representative traces of mIPSCs recorded from seizure-exposed and control cells. 1, 2 depict representative events (*left*) on an expanded time scale (*right*). Scale bar = 50 pA, 1 s and 50 pA, 20 ms, respectively. Number of recorded cells: new cells-seizures: 8 cells from 4 rats, new cells-control: 7 cells from 6 rats.

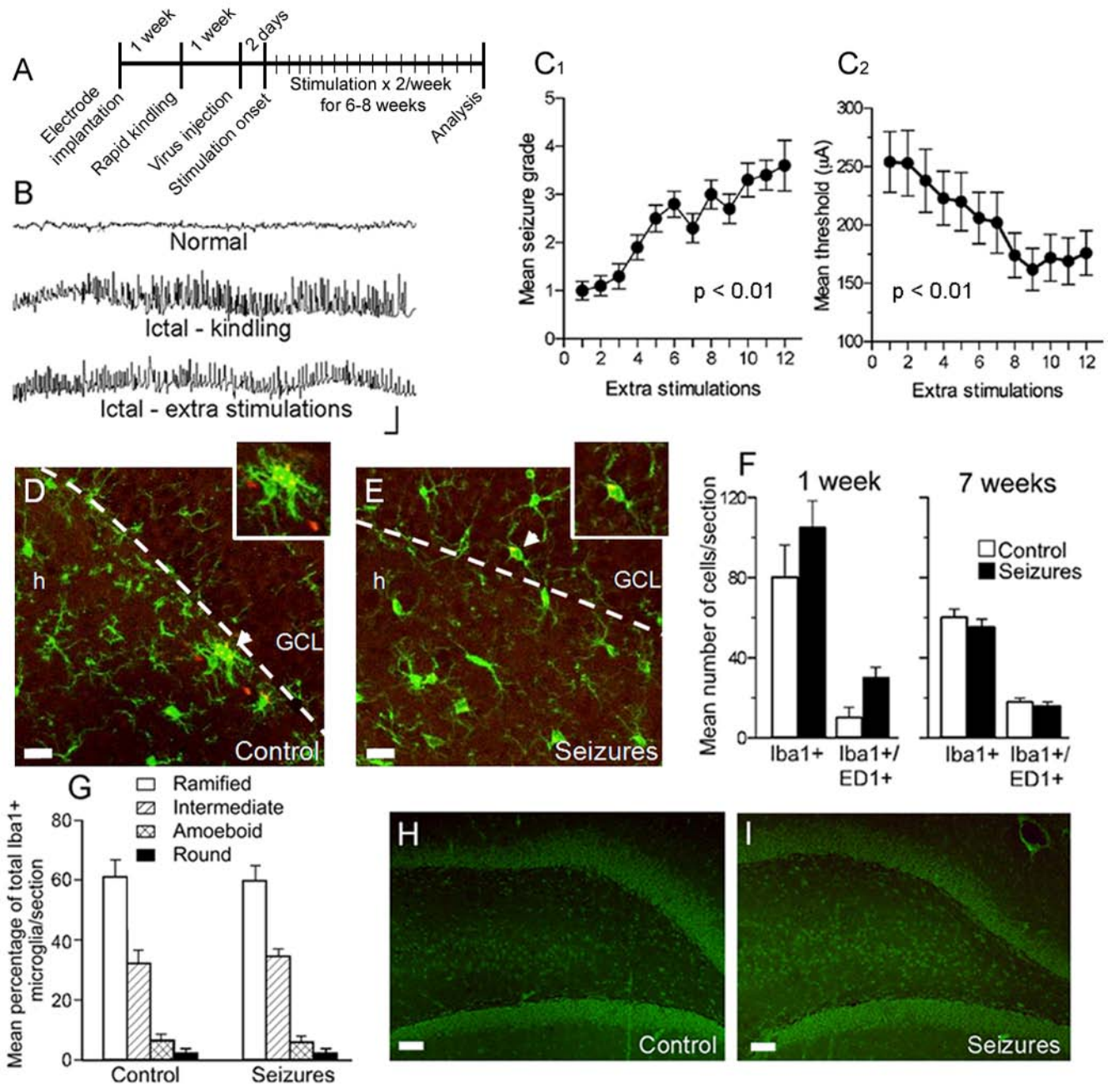
A
1 week
1 week
2 days
Stimulation x 2/week
for 6-8 weeks
Electrode implantation
Rapid kindling
Virus injection
Stimulation onset
Analysis
B
Normal
Ictal - kindling
Ictal - extra stimulations
C1
Mean seizure grade
p < 0.01
Extra stimulations
C2
Mean threshold (μA)
p < 0.01
Extra stimulations
D
h
GCL
Control
E
h
GCL
Seizures
F
1 week
7 weeks
Control
Seizures
Mean number of cells/section
Iba1+
Iba1+/ ED1+
G
Ramified
Intermediate
Amoeboid
Round
Mean percentage of total Iba1+ microglia/section
Control
Seizures
H
Control
I
Seizures

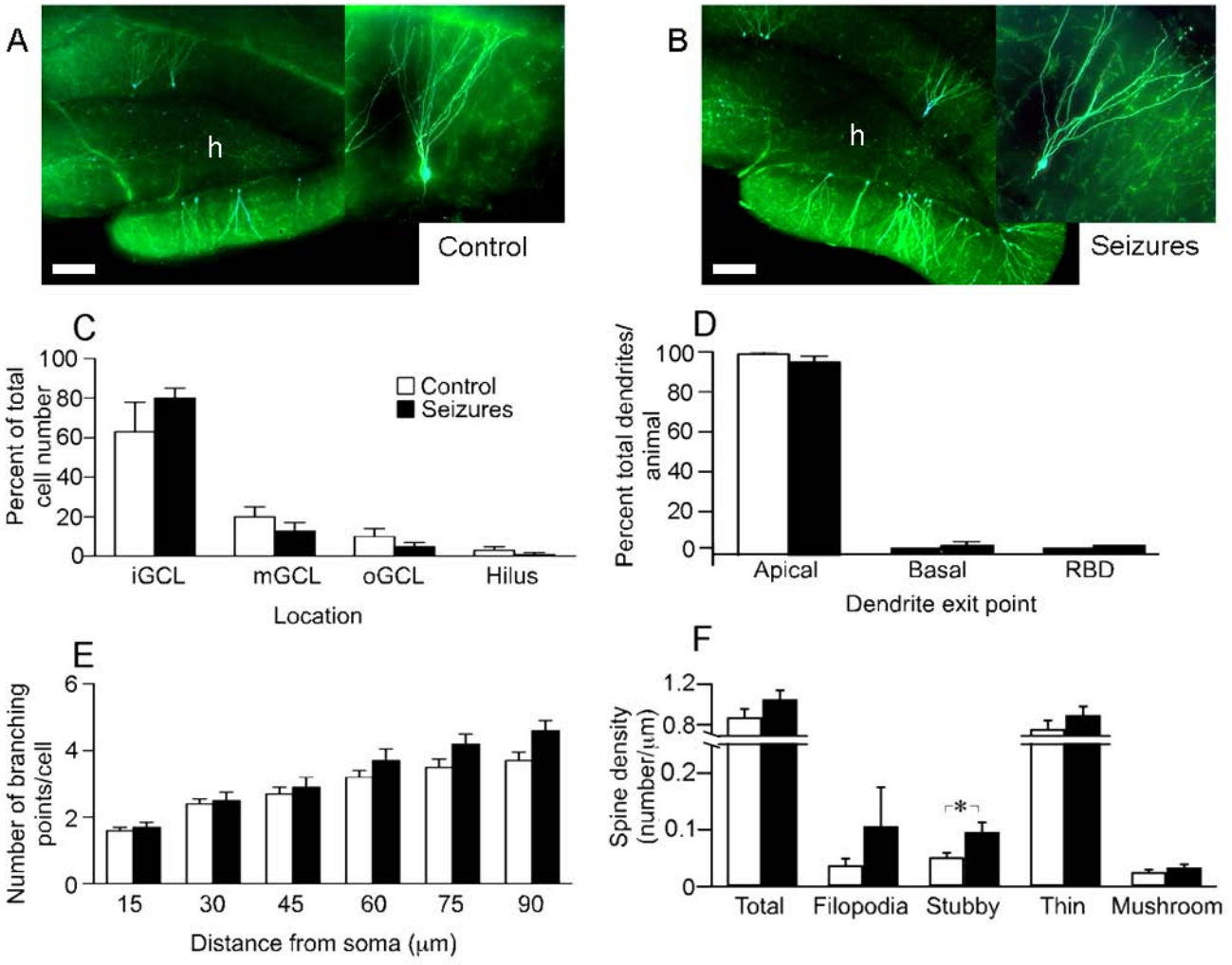
A
h
Control
B
h
Seizures
C
Percent of total cell number
100
80
60
40
20
0
Control
Seizures
iGCL
mGCL
oGCL
Hilus
Location
D
Percent total dendrites/ animal
100
80
60
40
20
0
Apical
Basal
RBD
Dendrite exit point
E
Number of branching points/cell
6
4
2
0
15
30
45
60
75
90
Distance from soma (μm)
F
Spine density (number/μm)
1.2
0.8
0.2
0.1
0
*
Total
Filopodia
Stubby
Thin
Mushroom
G
Control
H
Seizures

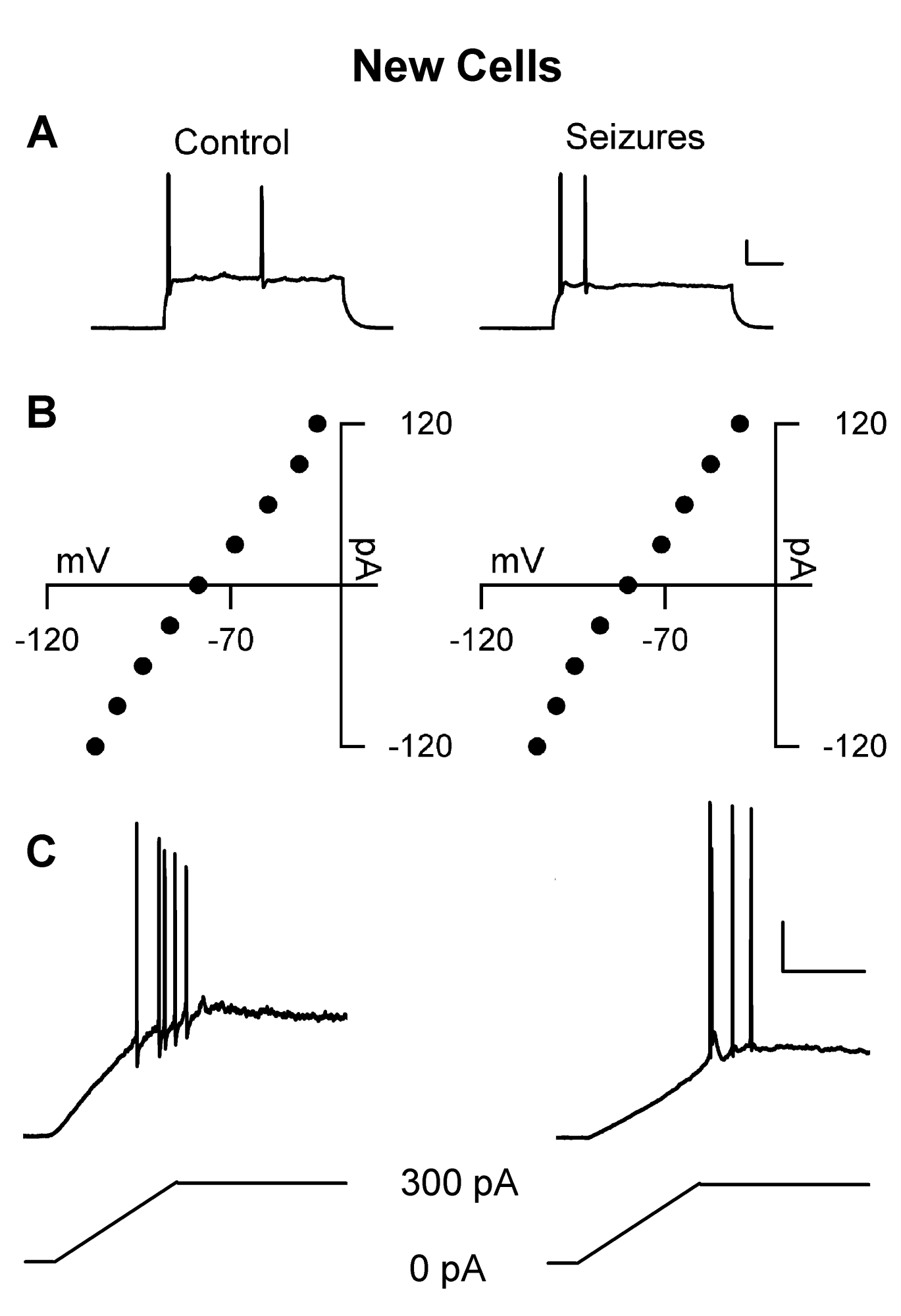
New Cells
A
Control
Seizures
B
120
mV
pA
-120
-70
-120
120
mV
pA
-120
-70
-120
C
300 pA
0 pA

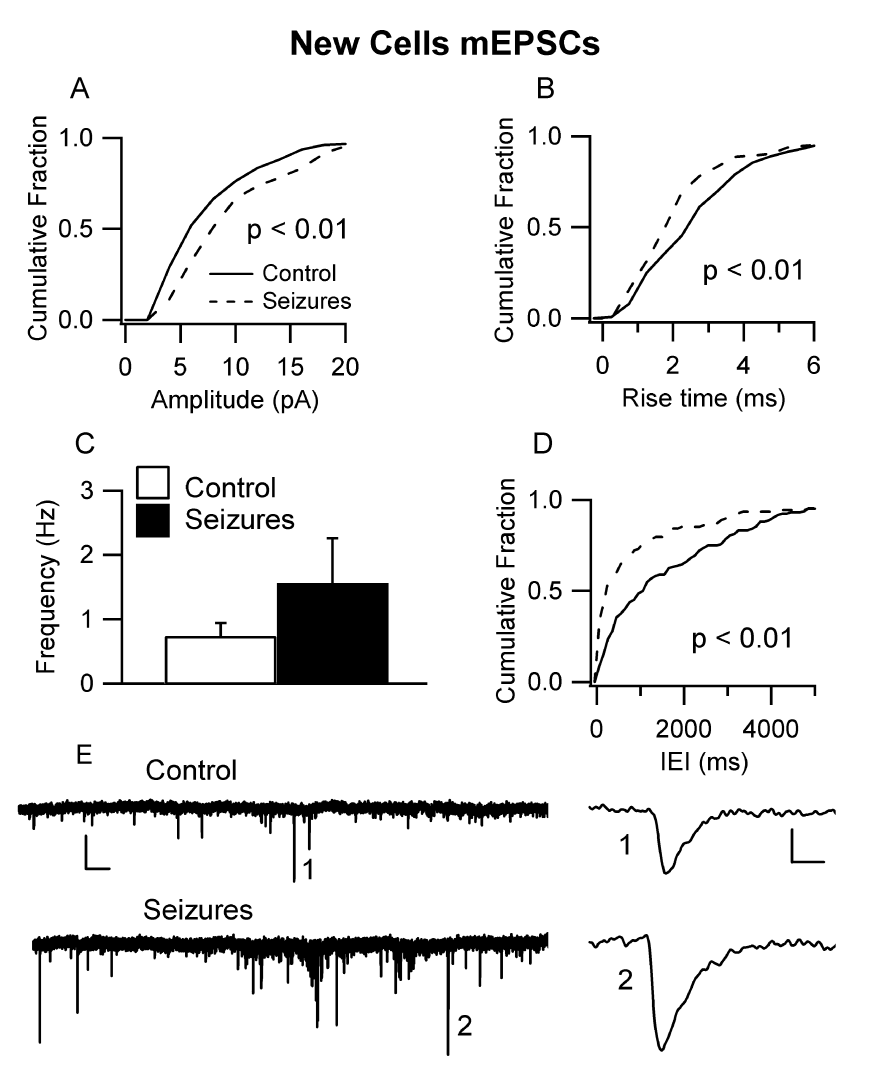
New Cells mEPSCs
A
Cumulative Fraction
1.0
0.5
0.0
p < 0.01
Control
Seizures
0
5
10
15
20
Amplitude (pA)
B
Cumulative Fraction
1.0
0.5
0.0
p < 0.01
0
2
4
6
Rise time (ms)
C
Frequency (Hz)
3
2
1
0
Control
Seizures
D
Cumulative Fraction
1.0
0.5
0.0
p < 0.01
0
2000
4000
IEI (ms)
E
Control
1
Seizures
2
1
2

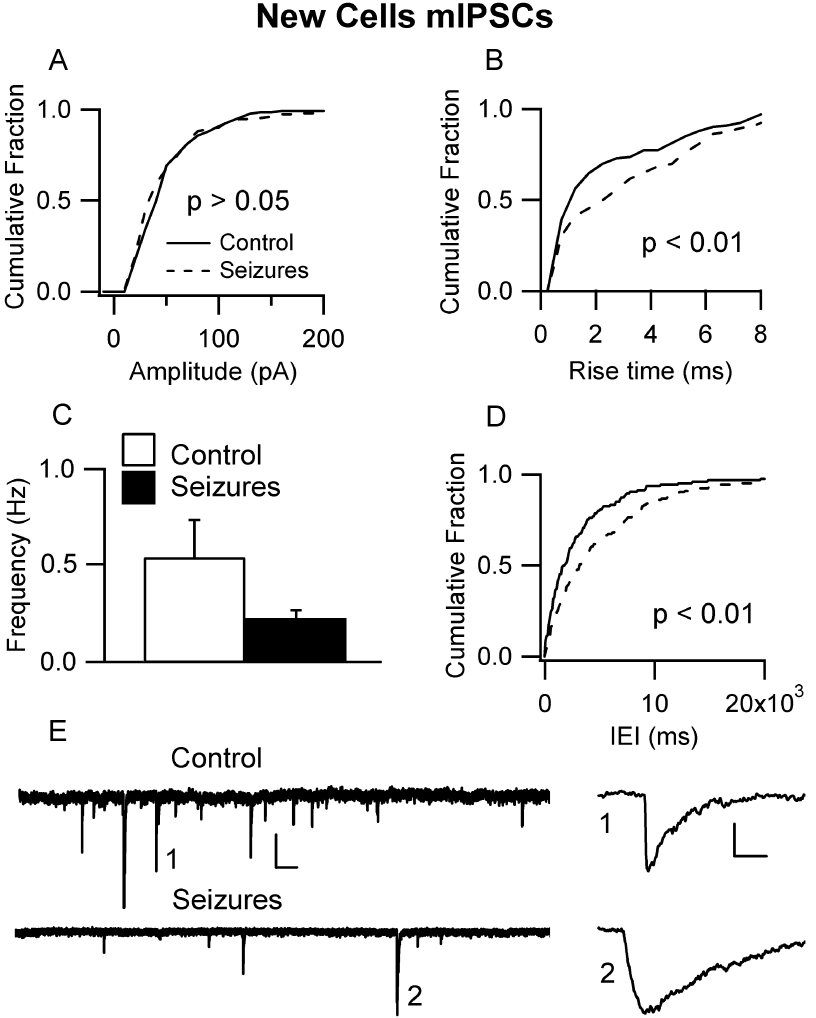
New Cells mIPSCs
A
Cumulative Fraction
1.0
0.5
0.0
p > 0.05
Control
Seizures
0
100
200
Amplitude (pA)
B
Cumulative Fraction
1.0
0.5
0.0
p < 0.01
0
2
4
6
8
Rise time (ms)
C
Control
Seizures
Frequency (Hz)
1.0
0.5
0.0
D
Cumulative Fraction
1.0
0.5
0.0
p < 0.01
0
10
20x10^3
IEI (ms)
E
Control
1
Seizures
2
1
2

Supplementary Material

Supplementary Figure 1. Electrical status epilepticus, but not rapid kindling, results in a shift of microglia towards a more activated morphological phenotype at 1 week after the epileptic insult. Iba1+ microglia exhibit significant decrease in ramified and increase in intermediate phenotype in eSE animals compared to seizure-exposed and control animals (*, $p < 0.05$, **, $p < 0.01$, one-way ANOVA with Bonferroni *post-hoc* test). Means ± SEM.

Supplementary Figure 2. Mature cells exposed to repeated seizures without inflammation exhibit altered excitatory input in the absence of network activity. Cumulative fraction curve showing decreased amplitude and slower 10-90% rise time of mEPSCs in mature cells from seizure-exposed compared to mature cells in control animals after action potential blockade with TTX (*A, B*). No change in mean event frequency (Student's unpaired t-test, $p > 0.05$), but shorter IEI of mEPSCs in mature cells exposed to seizures compared to control mature cells (*C, D*) (Kolmogorov-Smirnov test). *E*, Representative traces of mEPSCs in seizure-exposed and control cells. 1, 2 depict representative events (*left*) on an expanded time scale (*right*). Scale bar = 10 pA, 1 s and 10 pA, 5 ms, respectively. Number of recorded cells: mature cells-seizures: 8 cells from 5 rats, mature cells-control: 8 from 5 rats.

Supplementary Figure 3. Mature cells exposed to repeated seizures without inflammation exhibit slower 10-90% rise time but no change in inhibitory input in the absence of network activity.

Cumulative fraction curves showing no change in amplitude and slower 10-90% rise time of mIPSCs in mature cells from seizure-exposed compared to control animals after action potential blockade with TTX (*A, B*). No change in mean event frequency (Student's unpaired t-test, $p > 0.05$) or IEI of mIPSCs in mature cells exposed to seizures compared to control mature cells (*C, D*). (Kolmogorov-Smirnov test). *E,* Representative traces of mIPSCs recorded from seizure-exposed and control cells. 1, 2 depict representative events (*left*) on an expanded time scale (*right*). Scale bar = 50 pA, 1 s and 50 pA, 20 ms, respectively. Number of recorded cells: mature cells-seizures: 9 cells from 6 rats, mature cells-control: 8 cells from 7 rats.

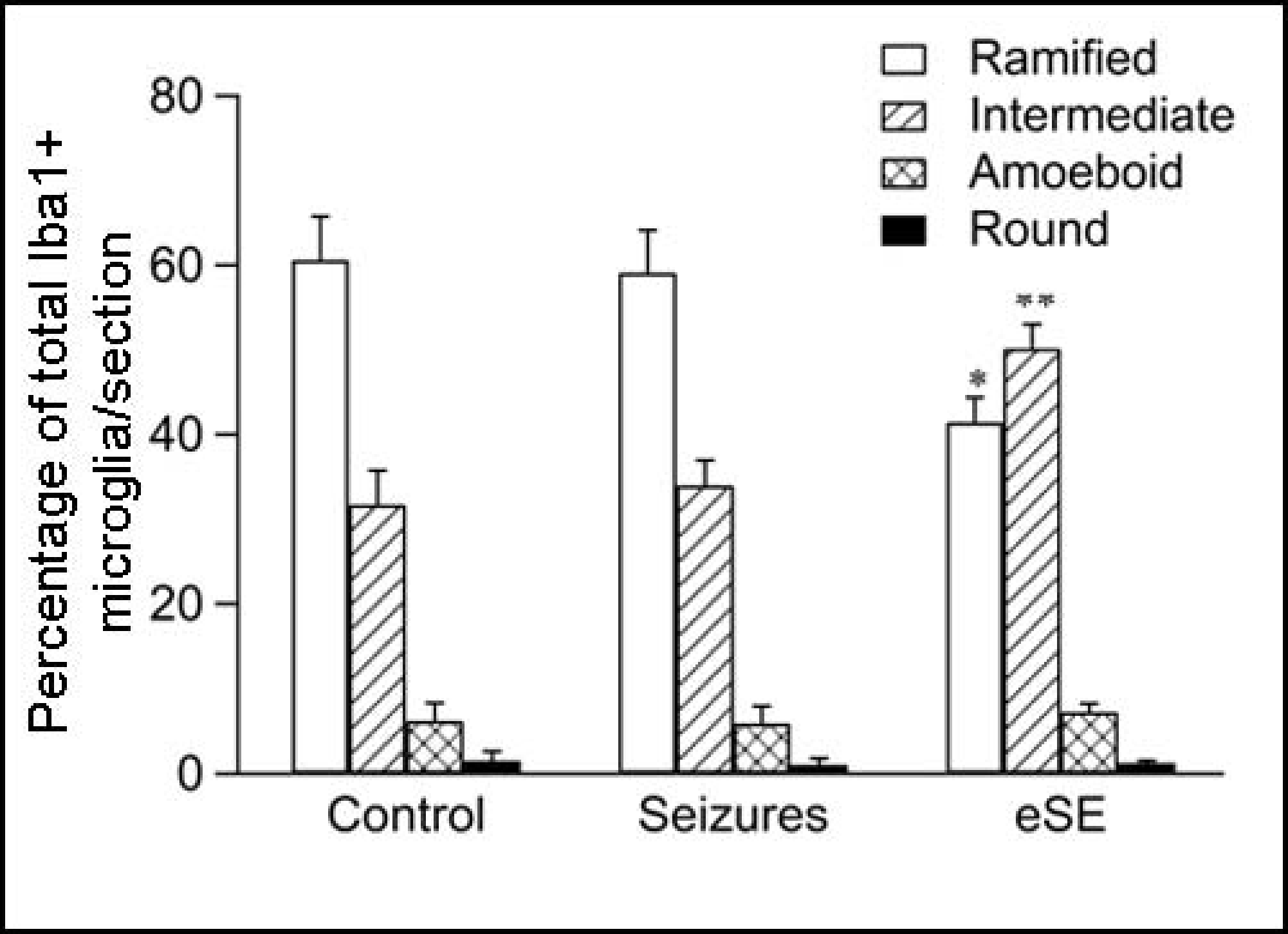
Ramified
Intermediate
Amoeboid
Round
Percentage of total Iba1+ microglia/section
80
60
40
20
0
*
**
Control
Seizures
eSE

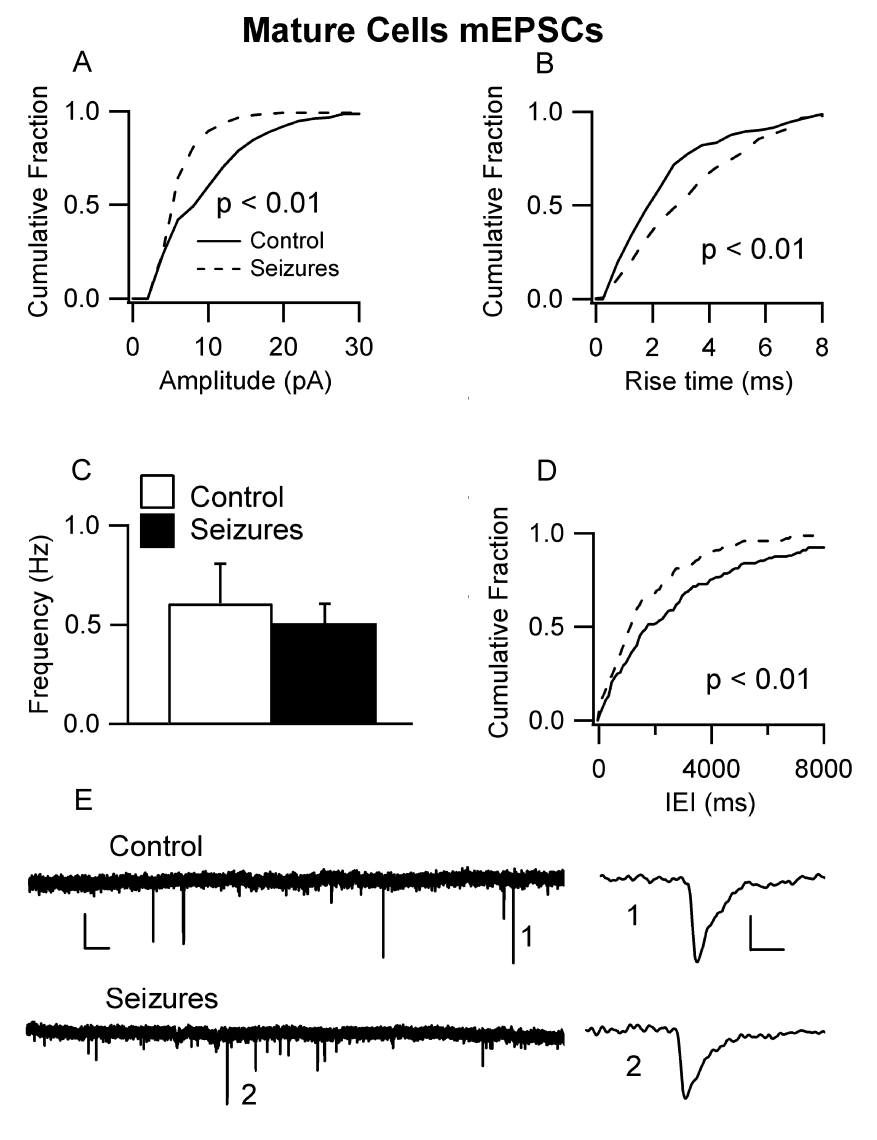
Mature Cells mEPSCs
A
Cumulative Fraction
1.0
0.5
0.0
p < 0.01
Control
Seizures
0
10
20
30
Amplitude (pA)
B
Cumulative Fraction
1.0
0.5
0.0
p < 0.01
0
2
4
6
8
Rise time (ms)
C
Control
Seizures
Frequency (Hz)
1.0
0.5
0.0
D
Cumulative Fraction
1.0
0.5
0.0
p < 0.01
0
4000
8000
IEI (ms)
E
Control
1
1
Seizures
2
2

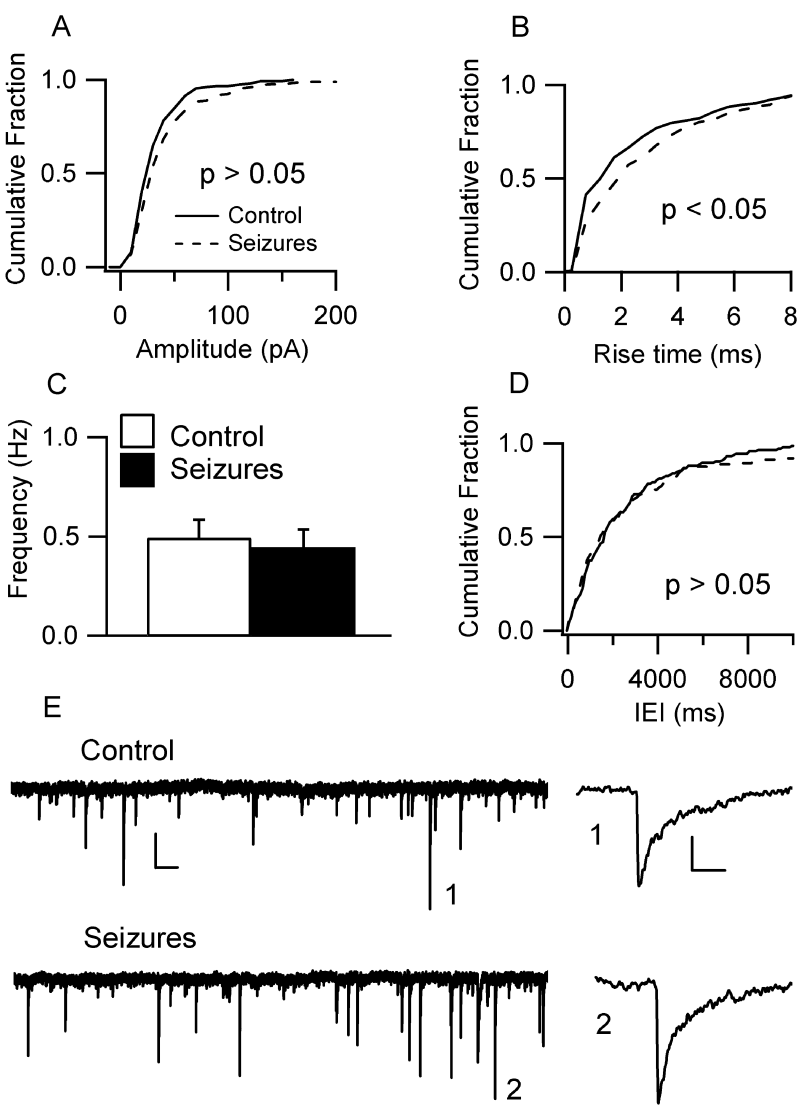
Mature Cells mIPSCs
A
Cumulative Fraction
1.0
0.5
0.0
p > 0.05
Control
Seizures
0
100
200
Amplitude (pA)
B
Cumulative Fraction
1.0
0.5
0.0
p < 0.05
0
2
4
6
8
Rise time (ms)
C
Frequency (Hz)
1.0
0.5
0.0
Control
Seizures
D
Cumulative Fraction
1.0
0.5
0.0
p > 0.05
0
4000
8000
IEI (ms)
E
Control
1
1
Seizures
2
2